Loschmidt-echo approach to error estimation in Krylov-subspace approximation

Julian M. Ruffinelli, Emiliano M. Fortes, Diego A. Wisniacki, and Martín Larocca

Phys. Rev. A **106**, 042423 — Published 18 October 2022

DOI: 10.1103/PhysRevA.106.042423

Loschmidt echo approach to Krylov-subspace approximation error estimation

Julian M. Ruffinelli, Emiliano M. Fortes, and Diego A. Wisniacki
Departamento de Física "J. J. Giambiagi" and IFIBA, FCEyN, Universidad de Buenos Aires, 1428 Buenos Aires, Argentina

Martín Larocca
Theoretical Division, Los Alamos National Laboratory, Los Alamos, New Mexico 87545, USA and
Departamento de Física "J. J. Giambiagi" and IFIBA, FCEyN, Universidad de Buenos Aires, 1428 Buenos Aires, Argentina

The Krylov subspace method is a traditional approach to approximate quantum evolution, allowing to treat systems with large Hilbert spaces. Despite its popularity, current bounds typically overestimate the error, which translates into more expensive simulation routines. In this paper, we tackle this problem by realizing that the error can be understood as a Loschmidt echo in a 1-D non-interacting tight-binding Hamiltonian. We show that the different time-regimes of the approximation can be understood using simple physical ideas. More importantly, we obtain computationally cheap error bounds that describe with high precision the actual error in the approximation.

I. INTRODUCTION

Quantum devices capable of transmitting and processing information have been established recently [1]. Laboratories around the world are in the race to develop increasingly accurate quantum devices. To carry out this successfully, it is necessary to test their operation on classical devices. For this reason, it is important to have efficient classical algorithms to perform quantum simulations [2, 3].

Several approaches for the efficient computation of quantum time-evolution have been proposed in the literature [4–8]. The cost of the simulation usually depends on the specifics of the system, e.g. the initial state, or on the information that we want to know about the dynamics. For example, the cost of the simulation can be greatly reduced if the amount of entanglement developed by the system remains bounded [7, 8]. Less restrictive are the well-known Krylov-subspace methods, constructed to provide approximations to the action of the exponential of a matrix on a vector. In the context of quantum simulation, the mechanics of the approximation is the following: an initial state in a (possibly very) large Hilbert space is first mapped to an effective subspace, the Krylov subspace, that captures the most relevant features of the dynamics. Within this low-dimensional subspace, time evolution is (cheaply) computed. Finally, the evolved state is mapped back to the large Hilbert space. Besides quantum simulation, the method has other important applications like solving systems of ordinary differential equations, large-scale linear systems and more [9, 10]

The core challenge in Krylov-subspace methods is to keep the error at low values and, thus, achieve a precise evolution. For this reason, it is desirable to predict the time regime in which the error will remain less than a given predetermined tolerance. This problem has been approached in several ways in the literature [11–15, 17, 18], and the provided bounds generally overestimate the error (significantly). In the seminal paper [11], Park and Light use the fact that the dynamics in the reduced subspace is that of an effective 1d lattice with a tridiagonal Hamiltonian. An initial state localized at one end starts spreading and the error in the method is approximated by the population at the other end of the chain. Later, Saad [12] derived computable estimates of the error using an expansion in the Krylov subspace exploiting the Lanczos algorithm. Other error bounds include involved computations making it difficult to use in an operational way [14].

The goal of this paper is to find tight and computationally inexpensive error bounds for the approximation error in Krylov schemes. We take advantage of a simple observation: the error can be regarded as a Loschmidt echo in which both the forward and backward evolutions are given by 1-D non-interacting tight-binding Hamiltonians. In a virtual chain, we have an initial state that is localized at one end. The error is related to an echo between evolutions in a D site chain and a trimmed $N << D$ chain, where N is the dimension of the truncated Krylov subspace used for the approximation. This analogy allows us to describe the time-regimes of the error using Loschmidt echo theory. In particular, we show that the error remains negligible up to some time at which it starts building up exponentially. This time is related to the tail of the travelling wave-packet hitting the end of the virtual chain [11]. The core of our proposal is that, in this regime, the error can be captured remarkably well by replacing the full-size evolution with the one of a chain with a single extra site. As we show, this provides an accurate and cheap bound for the error. To motivate this behaviour, we analytically solve for the bound in the case in which the 1-D non-interacting tight-binding Hamiltonian has homogeneous diagonal and off-diagonal elements. We test this solution in a one-dimensional Ising spin chain with a transverse magnetic field. Finally, we give some physical insight that explains why this simple model works in the general case.

The paper is organized as follows. In Sec. II, we in-

troduce the general framework of the Krylov-subspace method for quantum time evolution. In Sec. III, we describe the different time-regimes of the error, focusing on the analogy with Loschmidt echo dynamics under 1-D non-interacting tight-binding Hamiltonians. In Sec. IV, we use the connection between the error and the Loschmidt echo of 1-D non-interacting tight-binding Hamiltonians to propose a bound that describes extremely well the inaccuracy of the approximate evolution in the Krylov subspace. Finally, in Sec. V, we offer some final remarks. Appendix A provides a brief description of Lanczos algorithm and Appendix B includes details of the system used for the numerical simulations, a one-dimensional Ising spin chain with a transverse magnetic field. Appendix C offers a study of the scaling of the time regimes with the size of the Krylov subspace and Appendix D derives results for the robustness of estimating the error using an approximation for the next hopping term. In Appendix E, the error bound is analytically solved for the simple case in which the 1-D non-interacting tight-binding Hamiltonian has homogeneous diagonal and non-diagonal elements.

II. THE KRYLOV-SUBSPACE METHOD

Let us start by reviewing the so-called Krylov-subspace method for approximating quantum dynamics. Consider a state $|\psi\rangle$ in a D-dimensional complex Hilbert space $\mathcal{H} = \mathbb{C}^D$, that evolves under a time-independent Hamiltonian $H \in \mathrm{End}(\mathcal{H})$. The N-dimensional Krylov subspace associated with $|\psi\rangle$ and H is given by

$$\mathcal{K}_N = \mathrm{span}\{|\psi\rangle, H|\psi\rangle, \ldots, H^{N-1}|\psi\rangle\}. \tag{1}$$

Here, without loss of generality, we consider that H and $|\psi\rangle$ share no symmetries, i.e. such that $\mathcal{K}_D = \mathcal{H}$. If they did share some symmetry, time evolution would occur constrained to its respective subspace $\mathcal{H}_j \subset \mathcal{H}$. In this case, the problem is redefined to the one belonging within that subspace, e.g. $\mathcal{H} \leftarrow \mathcal{H}_j$.

The Krylov approach aims at approximating the time-evolved state $|\psi(t)\rangle$ with the best element $|\psi_N(t)\rangle \in \mathcal{K}_N$. To do so, we first have to build an orthonormal basis for $\mathcal{K}_N$, which we denote $B_N = \{|v_0\rangle \equiv |\psi\rangle, \ldots, |v_{N-1}\rangle\}$. This is usually done using Lanczos's algorithm, a sort of Gram-Schmidt procedure that harnesses the fact that orthonormalization only needs to be enforced with respect to the last two vectors in the basis (see Appendix A). Using B_N, we approximate the time-evolved state by projecting into $\mathcal{K}_N$[1],

$$\begin{aligned} |\psi(t)\rangle = e^{-iHt}|\psi\rangle &\approx \mathbb{P}_N e^{-iHt}\mathbb{P}_N|\psi\rangle \\ &= \mathbb{V}_N^\dagger e^{-iT_N t}\mathbb{V}_N|\psi\rangle \\ &\equiv |\psi_N(t)\rangle\,. \end{aligned} \tag{2}$$

Here, $T_N = \mathbb{V}_N H \mathbb{V}_N^\dagger$ is the Hamiltonian H reduced to the Krylov subspace $\mathcal{K}_N$, and

$$\mathbb{V}_N^\dagger = \begin{bmatrix} \vdots & \vdots & \vdots \\ |v_0\rangle, & |v_1\rangle, & , |v_{N-1}\rangle \\ \vdots & \vdots & \vdots \end{bmatrix} \tag{3}$$

and $\mathbb{P}_N = \mathbb{V}_N^\dagger \mathbb{V}_N$ are the reduction-to-the-subspace operator and projector, respectively. By definition, $\mathbb{V}_N$ maps given initial state into the first coordinate vector of an effective N-dimensional system, $\mathbb{V}_N|\psi\rangle = (1, 0, \cdots, 0)^T \equiv |0\rangle_N$. It is especially relevant to notice that the Hamiltonian reduced to a Krylov subspace is tridiagonal

$$T_N = \begin{pmatrix} \alpha_1 & \beta_1 & 0 & \cdots & 0 \\ \beta_1 & \alpha_2 & \beta_2 & \cdots & 0 \\ 0 & \beta_2 & \alpha_3 & \cdots & 0 \\ \vdots & \vdots & \vdots & \ddots & \vdots \\ 0 & 0 & 0 & \cdots & \alpha_N, \end{pmatrix} \tag{4}$$

and, thus, the system in the Krylov basis (henceforth, the *effective* system) has the form of a 1-D non-interacting tight-binding model. An initial state localized in one end of an effective chain evolves according to T_N (i.e. with onsite potential α_i and hopping amplitude β_i at the ith site) propagating the excitation and populating the rest of the lattice (see Fig. 1(b) for a schematic representation). Finally, $\mathbb{V}_N^\dagger$ maps the effective evolved state back to full Hilbert space. The efficiency of the method resides in the fact that the time evolution is solved with very few computational costs in the reduced space, i.e. one replaces the exponential of a $D \times D$ Hermitian matrix H with the much more economical exponential of a $N \times N$ symmetric tridiagonal T_N. Of course, the assumption is that $N << D$.

The challenge in this approximate evolution scheme is to keep the error bounded by a given tolerance. This has been studied in different ways for more than three decades [11–15, 17, 18]. In the next Section, we show that the error as a function of time has regimes that can be well understood using physical ideas based on Loschmidt echo theory and diffusion in a 1-D non-interacting tight-binding model [19].

[1] See Fig. 1 (a) for a schematic representation of the method

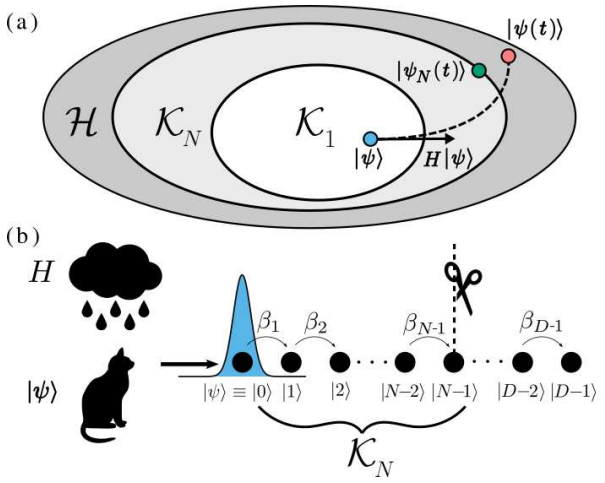

Figure 1. Schematic Krylov Approximation: (a) An initial state $|\psi\rangle$ (blue circle) evolves under Hamiltonian H, drawing some trajectory on Hilbert space $\mathcal{H}$ (dashed line). At time t, the evolved state is $|\psi(t)\rangle$ (red circle). The Krylov approach consists in approximating this state with $|\psi_N(t)\rangle$, its projection into the Krylov subspace $\mathcal{K}_N$ (green circle), defined in Eq. (1). (b) The dynamics of $|\psi\rangle$ under H, from the Lanczos Basis perspective, corresponds to the diffusion of an initial state $|0\rangle$ that is completely localized at the leftmost end of a virtual tight-binding chain. Here, the off-diagonal elements of Lanczos tridiagonal matrix, β_i, act as hopping amplitudes between neighbouring sites and the diagonal elements α_i as local onsite potentials (not depicted in the image). Using a truncated Lanczos basis can be regarded as "cutting" the chain at site N.

III. TIME REGIMES OF THE ERROR

Let us review the time regimes of the error in the Krylov-subspace method. Such error is given by the instantaneous infidelity between exact and approximate evolved states

$$\epsilon_N(t) = 1 - |\langle\psi_N(t)|\psi(t)\rangle|^2. \tag{5}$$

Any actual implementation of the approximation method has to keep track of this error. Notoriously, its exact computation is out of the question because it involves solving the problem one is trying to approximate, e.g. constructing $|\psi(t)\rangle$.

A closer inspection of Eq. (5) allows for an interesting interpretation. Rewriting the overlap as,

$$\begin{aligned}
|\langle\psi_N(t)|\psi(t)\rangle|^2 &= \left|\langle\psi|\mathbb{V}_N^\dagger e^{iT_N t}\mathbb{V}_N e^{-iHt}|\psi\rangle\right|^2 \\
&= \left|\langle\psi|\mathbb{V}_N^\dagger e^{iT_N t}\mathbb{V}_N\mathbb{V}_D^\dagger e^{-iT_D t}\mathbb{V}_D|\psi\rangle\right|^2 \\
&= \left|\langle\psi|\mathbb{V}_D^\dagger e^{i\tilde{T}_N t}\mathbb{V}_D\mathbb{V}_D^\dagger e^{-iT_D t}\mathbb{V}_D|\psi\rangle\right|^2 \\
&= \left|\langle 0|e^{i\tilde{T}_N t}e^{-iT_D t}|0\rangle\right|^2,
\end{aligned} \tag{6}$$

where $\tilde{T}_N = \mathbb{V}_D\mathbb{P}_N H\mathbb{P}_N\mathbb{V}_D^\dagger$ has the form

$$\tilde{T}_N = \left(\begin{array}{c|c} T_N & 0 \\ \hline 0 & 0 \end{array}\right), \tag{7}$$

it is noticed that $1-\epsilon_N(t)$ is described by a Loschmidt echo [19] on which both backwards and forward evolutions are described by tight-binding Hamiltonians. We start with $|0\rangle \equiv \mathbb{V}_D|\psi\rangle$, a completely localized state at one end of the virtual chain. This state evolves subject to T_D for some time t, then evolves backwards subject to $\tilde{T}_N$ (a perturbed T_D where the effective onsite potentials and hoppings of sites $N+1,\ldots,D$ are turned off) and is finally overlapped with the initial state $|0\rangle$.

The Loschmidt echo can measure the characteristic revival occurring after forward and backwards time evolutions generated by two slightly different Hamiltonians [19–21]. As far as we know, the case of tight-binding Hamiltonians has not been explicitly considered in the literature so far. We note that one of the evolutions happens with a chain of length D, while the other evolution corresponds to the case in which the chain gets clipped at site N (the hoppings and onsite potentials at the second part of the chain are set to zero, i.e. $\alpha_i = 0$ and $\beta_i = 0$ for $i = N+1,\ldots,D$).

To gain insight into the time regimes of the approximation, we show in Fig. 2 the Loschmidt echo $|\langle\psi_N(t)|\psi(t)\rangle|^2$ (top panel) and the error $\epsilon_N(t)$ (bottom panel) for an Ising spin chain with 10 sites and a transverse magnetic field (see Sec. IV for more details). From now on, we set $\hbar = 1$, such that energies are measured in units of the interaction strength J, and times in units of J^{-1}. The parameters of the chain are $J = 1$, $h_x = 1$ and $h_z = 0.5$, corresponding to a quantum chaotic case, i.e. the distribution of energy levels matches the one in Random Matrix Theory [22] (see Appendix B for more details). The initial state $|\psi\rangle$ is drawn randomly from the even subspace. Same results were obtained with initial states in the odd or even subspaces. We use a Krylov-subspace of $N = 30$ sites. We can see that the Loschmidt echo has two very different time regimes. Until the time of colition between the wave package and the end of the chain $t \approx t_{col}$, the echo remains roughly one and the approximate evolution faithfully captures the exact one. After this first "faithful" regime, an abrupt decrease is observed and from there on it decays in a monotonous way.

In this first time-regime $t < t_{col}$, where the echo practically does not change, the error has two relevant subregimes. First, until some time $t < t_{exp}$, the error is essentially zero. Then, at $t = t_{exp}$ the error suddenly starts to build-up exponentially. We can interpret this transition as the tail of the wave-packet starting to impact the end of the trimmed chain. The interval $t_{exp} \leq t \leq t_{col}$ precisely delimits the region where a proper approximation must happen to obtain a low error. We note that

the noisy plateau of $\varepsilon_N(t)$ for $t < t_{exp}$ is due to round-off errors in the floating-point arithmetic used in the computations.

In order to understand the time regimes of Fig. 2, we plot in Fig. 3 the square of the amplitudes in the Lanczos basis for both the exact and approximate evolved states of Eq. ((6)), i.e. $|\langle v_i|\psi_N(t)\rangle|^2$ and $|\langle v_i|\psi_D(t)\rangle|^2$ for $i = 1,\ldots,N$ and $i = 1,\ldots,D$, respectively. For the rest of the paper, we call the amplitudes $\langle v_i|\psi_K(t)\rangle \equiv \psi_{K,i}(t)$, We provide snapshots of these virtual travelling wave-packets at times $t = 10$, 25, 45 and 70. As mentioned before, we start with localized states at one end of the effective tight-binding chain. In the first panel of Fig. 3, corresponding to time $t = 10$, both wave-packets are travelling to the right and are essentially equal. However, at $t = t_{exp} \approx 25$, the exponential tail reaches the site $N = 30$, and the error starts to build up rapidly. This process continues until $t = t_{col} \approx 42$, where one of the packets bounces with the end of its chain and starts returning to its original position. This difference in the behavior of the wave-functions is reflected in an abrupt decay of the echo (see Fig. 2). At $t = 60$ and $t = 80$, the wave packets continuously grow apart and become more and more orthogonal. Although here we have chosen to illustrate the regimes of the error using a quantum chaotic spin chain, similar behaviour is observed in the integrable setting (see Appendix B for more details). Furthermore, Appendix C provides a study of the scaling of the time regimes with the size of the Krylov subspace. We observe a quasi-linear scaling, indicating that the dynamics slightly deviates from that of a wave-packet propagating at a constant speed (where both t_{exp} and t_{col} would scale linearly).

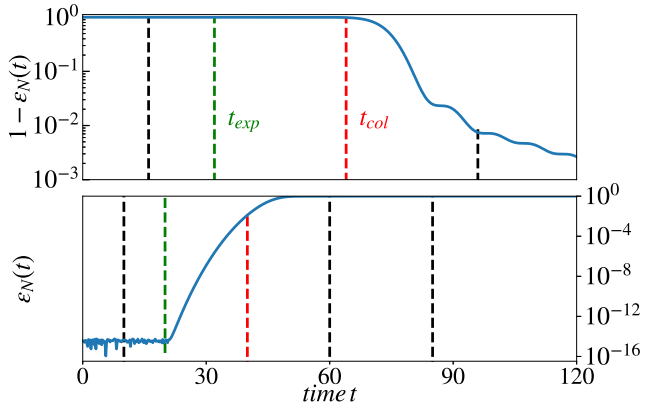

Figure 2. Time regimes of the echo. Loschmidt echo $|\langle\psi_N(t)|\psi(t)\rangle|^2 = |\langle\psi_N(t)|\psi_D(t)\rangle|^2$ (top panel) and error $\epsilon_N(t)$ (bottom panel) for an Ising spin chain with transverse magnetic field. We use $N = 30$ and $D = 2^L = 1024$, and the time is measure in units of J^{-1}. We have marked with dashed vertical lines the times that correspond to the snapshots shown in Fig. 3. We also highlight the relevant times t_{exp} and t_{col}. The initial state $|\psi\rangle$ is random state in the even subspace. See text for more details.

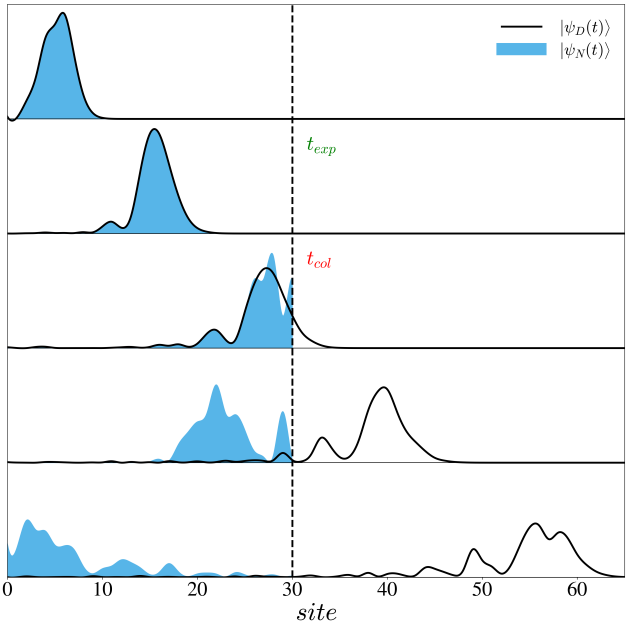

Figure 3. Time evolution of exact and approximate states in the Lanczos basis. We draw $|\langle v_i(t)|\psi_D(t)\rangle|^2 = |\psi_{D,i}(t)|^2$ (black line) and $|\langle v_i(t)|\psi_N(t)\rangle|^2 = |\psi_{N,i}(t)|^2$ (solid blue) at times $t = 10$, 25, 42, 60 and 80 (top to bottom). Remark: the representation in the figure takes a cubic interpolation between each site to smooth out the discrete sites effect for an easier visualization.

IV. FROM LOSCHMIDT ECHOES TO ERROR BOUNDS

In the previous section, we have shown that the error in the Krylov method can be seen as a Loschmidt echo. Let us now show how this description can help derive tight and computationally cheap bounds for the error, providing advantages for future implementations of the approximation method. In particular, we will focus on the time-regime that is relevant for such implementations: the one between t_{exp} and t_{col}. In this region, the travelling packet has its center between sites 1 and N, and only a small, exponentially suppressed population tail surpasses site N. With this in mind, we can ask ourselves: is it really necessary to consider the entire chain to describe the behavior of the error? Given that in the $[N+1, D]$ region we have exponentially suppressed populations, isn't it possible to capture the essential features of the error by considering instead an echo where we replace the full chain with one with $K = N + i$ sites, i.e. where i is a small number of extra sites? To answer

this question, we compare the echo $|\langle\psi_N(t)|\psi(t)\rangle|^2$ with $|\langle\psi_N(t)|\psi_K(t)\rangle|^2$ using $K=N+1$ and $K=N+5$ (see Fig. 4). Here, we can see that both cases (with one extra and five extra sites, respectively) accurately capture the important region between t_{exp} and t_{col} (shaded region of Fig. 4). In the inset of Fig. 4 we plot the error $\varepsilon_N^K(t) = 1 - |\langle\psi_N(t)|\psi_K(t)\rangle|^2$ in the shaded region to highlight this last conclusion. This remarkable fact, i.e. that only a single extra site is enough to capture the behaviour of the error in the relevant region, will be the main building block of our error bound proposal. Let us note that, although here we have used a spin chain model, the behavior appears to be the same for other fundamentally different systems [23]. Among others, we have confirmed this observation in random Hamiltonians that belong to the Gaussian Orthogonal Ensemble (GOE) and Gaussian Unitary Ensemble (GUE) [24] (see, for example, Appendix C).

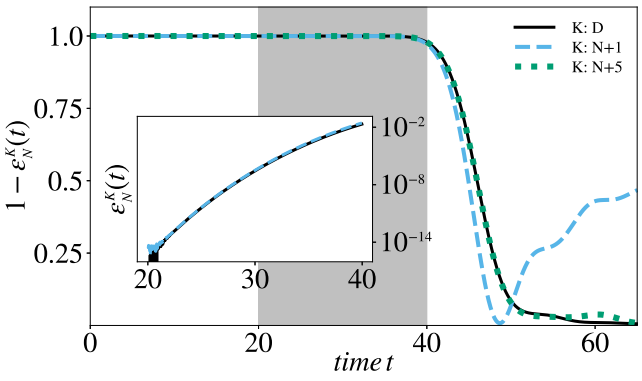

Figure 4. Loschmidt echo $|\langle\psi_N(t)|\psi_K(t)\rangle|^2$ with $K=N+1$ (light blue dashed line), $K=N+5$ (green dotted line) and D (black solid line). Here, we use $D=2^{10}$- dimensional Ising spin chain with transverse magnetic field. Inset: The error $\varepsilon_N^K(t)$ in the shaded region of the main plot.

Now, suppose we have computed the Krylov subspace $\mathcal{K}_N$ and want to estimate the error. As we have argued in the previous paragraph, one can effectively approximate the error with $|\langle\psi_N(t)|\psi_{N+1}(t)\rangle|^2$.To do so, one would have to perform an extra iteration of the Lanczos algorithm, i.e. to compute this extra site approximation $|\psi_{N+1}(t)\rangle$. Alternatively, it is possible to approximate the new site in the tight-binding chain without having to do such extra iteration. This is based on the fact that, as we show in Appendix D, the error in the β coefficient propagates quadratically into the approximation for the error of the Krylov method,

$$\varepsilon_{K+1}^K(t) \approx \left(\frac{\tilde{\beta}}{\beta}\right)^2 \left[1 - |\left\langle\tilde{\psi}_{K+1}(t)\middle|\psi_K(t)\right\rangle|^2\right], \qquad (8)$$

where $\left|\tilde{\psi}_{K+1}\right\rangle$ is the solution that corresponds to keeping the first K coefficients unchanged and replacing the last one with $\tilde{\beta}$.

A simple yet effective way of estimating the coefficients of this new site is to average over the previous sites. That is,

$$\alpha_{N+1} \approx \bar{\alpha} \equiv \frac{1}{N}\sum_1^N \alpha_i\,,$$
$$\beta_{N+1} \approx \bar{\beta} \equiv \frac{1}{N}\sum_1^N \beta_i\,. \qquad (9)$$

Finally, all the elements needed to test our error bound and compare it with the established ones from the literature, e.g. of Ref. [12], are ready. In Fig. 5, we show the ratio between the error bounds $\langle\varepsilon\rangle_N^{N+1}$ and the actual error ε_N of Eq. (5). We bracket the bound $\langle\varepsilon\rangle_N^{N+1}$ to denote that we use the averaged estimation of Eq. (9) for the coefficients of site $N+1$. In the inset of Fig. 5, we shade the region of the bound ε_N^{N+1} in which the elements α_{N+1} and β_{N+1} are the maximum o the minimum of α_i and β_i with $i=1,...N$. We also show the ratio of the bound of Ref. [12] with the actual error. We see that both the proposed bounds provide an overestimation that remains constant throughout the evolution, and is quite lower than Ref. [12].

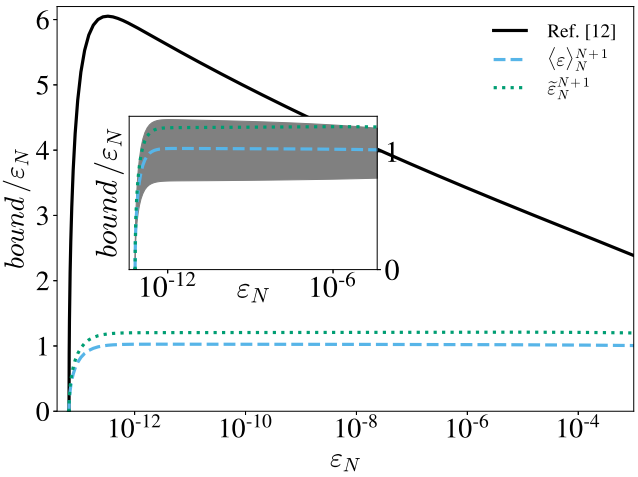

Figure 5. Ratio of the bounds $\langle\varepsilon\rangle_N^{N+1}$ (dashed line), $\tilde{\varepsilon}_N^{N+1}$ (dotted line) and the a posteriori bound of Ref. [12] (solid line) with the the actual error ε_N vs. ε_N. See text for more details.

Interestingly, the echo $|\langle\psi_N(t)|\psi_{N'}(t)\rangle|^2$ can be solved analytically in the particular case of homogeneous coefficients, $\forall i: \alpha_i = \alpha$ and $\forall i: \beta_i = \beta$, which corresponds to the Toeplitz tridiagonal matrix [25] (see Appendix E for the derivation). Using such analytical expression, we compute a new bound $\tilde{\varepsilon}_N^{N+1}$ (with a *tilde*) where we use Eq. (E6) with $\alpha=\bar{\alpha}$ and $\beta=\bar{\beta}$ in Eq. (9).

We finally show in Fig. 5 that this approximation also works very well.

V. CONCLUSIONS

In this work, we have established a connection between the behavior of the error in Krylov-subspace approximations for quantum simulation, and a Loschmidt echo between effective wave-packets travelling in effective tight-binding chains. One of such chains has D sites and the other one $N << D$. The packages start at the leftmost end of the chain, and for some time their profile is identical. Then, at $t \approx t_{exp}$, the tail of the *approximate* packet starts colliding with the end of the chain and bouncing back, while the *true* packet's tail continues its journey unaltered. This discrepancy causes errors to build-up exponentially. At a later time,$t \approx t_{col}$, the center of this packet arrives at the end of the chain and bounces back. Here, the error reaches significant values and the echo forever departs from unity. Hereafter, the packages travel in opposite directions and they become ever more orthogonal.

In practice, any approximation method must be accompanied by an efficient and accurate error estimator. Yet, error estimation for Krylov-subspace method has been an elusive subject for more than 30 years [11–15, 17, 18]. Thus, the Loschmidt echo picture offers, apart from a nice physical insight on the mechanics of the error, an elegant and simple solution to the error tracking problem. Remarkably, we show that one can capture with extreme precision the behaviour of the error in the relevant region, without having to incur extra computations.

Typical implementations of Krylov-subspace methods involve a time-stepping schedule [15]. The reason for this is that Lanczos's Algorithm suffers from instabilities when Krylov basis is large. Thus, the common workaround is to approximate the evolution using an iterative approach: the actual trajectory in Hilbert space is efficiently followed using a sequence of patches [16]. That is, we build a Krylov-subspace, evolve for a small-time, map back and start over. In this framework, our error bounds provide a cheap and accurate way of computing optimal time intervals for the time-stepping schedule. An open-source implementation in Python of the Krylov evolution using the error bound developed in this paper can be found in the GitHub repository at https://github.com/emilianomfortes/krylovsolver.

ACKNOWLEDGEMENTS

The work was partially supported by CONICET (PIP 112201 50100493CO), UBACyT (20020130100406BA), ANPCyT (PICT-2016-1056), and Unitary Fund. ML was supported by the U.S. Department of Energy (DOE), Office of Science, Office of Advanced Scientific Computing Research, under the Accelerated Research in Quantum Computing (ARQC) program as well as under the Quantum Computing Application Teams program.

Appendix A: Lanzcos method

The Lanczos method (see Algorithm 0) is a well known strategy for the construction of $B_N = \{|v_0\rangle, \ldots, |v_{N-1}\rangle\}$, an orthonormal basis spanning the Krylov subspace $\mathcal{K}_N$. One of the most appealing features of this approach is that, unlike e.g. a Gram-Schmidt procedure where orthonormalization at each step involves the whole current basis, the new candidate vector $|x_j\rangle$ only needs to be orthonormalized with respect to the previous two basis vectors $|v_{j-1}\rangle$ and $|v_{j-2}\rangle$. The reason for this is that the Hamiltonian, by construction, is tridiagonal in the Lanczos Basis (see Eq. (4)).

Algorithm1 Lanczos Algorithm. Receives state $|\psi\rangle$ and Hamiltonian H and returns a set of N orthonormal vectors $\{|v_i\rangle\}$ spanning the Krylov subspace $\mathcal{K}_N$.

$|v_0\rangle = |\psi\rangle$ (assume normalized)
$|x_1\rangle = H|\psi\rangle$
$\alpha_1 = \langle x_1|v_0\rangle$ (the component of $|x_1\rangle$ in $|v_0\rangle$)
$|w_1\rangle = |x_1\rangle - \alpha_1 |v_0\rangle$
for $j = 1, 2, \ldots$ **do**
    $\beta_j = \sqrt{\langle \omega_j | \omega_j \rangle}$
    if $\beta_j > 0$ **then**
        $|v_j\rangle \leftarrow \frac{1}{\beta_j} |\omega_j\rangle$.
    else
        break
    $|x_{j+1}\rangle = H|v_j\rangle$
    $\alpha_{j+1} = \langle x_{j+1}|v_j\rangle$
    $|\omega_{j+1}\rangle = |x_{j+1}\rangle - \alpha_{j+1}|v_j\rangle - \beta_j |v_{j-1}\rangle$

Appendix B: Ising spin chain in a transverse magnetic field

Let us describe the system used in the numerical simulations. Consider a 1D Ising spin chain with transverse magnetic field and open boundary conditions, described by,

$$H = \sum_{k=1}^{L} (h_x \hat{\sigma}_k^x + h_z \hat{\sigma}_k^z) - J \sum_{k=1}^{L-1} \hat{\sigma}_k^z \hat{\sigma}_{k+1}^z, \qquad \text{(B1)}$$

where L is the total number of spin-1/2 sites of the chain, $\hat{\sigma}_k^j$ to the Pauli operator at site $k \in \{1, 2, ..., L\}$ with direction $j \in \{x, y, z\}$ and J represents the interaction

strength within the site k and $k+1$. The parameters h_x and h_z are, respectively, the strength of the magnetic field in the (transverse) x direction, and in the (parallel) z direction. We set $\hbar = 1$, such that energies are measured in units of the interaction strength J, and times in units of J^{-1}.
The Hamiltonian of Eq. (B1) has parity conservation. The parity is defined through the permutation operators $\hat{\Pi} = \hat{P}_{1,L}\hat{P}_{2,L-1}\dots\hat{P}_{L/2-1,L/2+1}$ for a chain of odd length L and for the even case it is analogous. The spanned space is divided into odd and even subspaces with dimension $D = D^{even} + D^{odd}$ ($D^{even/odd} \approx D/2$). This symmetry must be taken into account for studying the effect of quantum chaos transition. While this model is integrable in the limit of $h_z \gg h_x$ and $h_x \gg h_z$, it exhibits quantum chaos when the longitudinal and the transverse field are of comparable strength. In Fig.2 we illustrate the behavior of the error $\epsilon_N(t)$ when the system is in the quantum chaos regime, that is, the statistical distribution of eigenenergies and eigenfunctions are well described by Random matrix theory [22]. For the computations, we fix $h_x = 1$ and we consider the most chaotic case $h_z = 0.5$.

The question now is to establish what happens when the system is in the integrable regime. For this reason, in Fig. 6 we plot the error for an Ising spin chain with $L = 10$ sites with $J = 1$, $h_x = 1$ and $h_z = 0$ and $h_z = 10$ which corresponds to integrable cases, that is, the energy levels follows a Poisson distribution. We can see that the error in both limits has the same behaviour that the chaotic case of $h_z = 0.5$ (which we also plot for convenience).

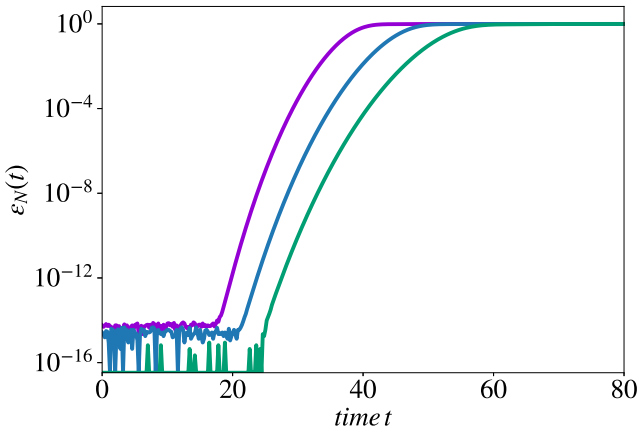

Figure 6. $\epsilon_N(t)$ for an Ising spin chain with transverse magnetic field. We use $N = 30$, $D = 2^L = 1024$ $J = 1$, $h_x = 1$ and $h_z = 0$ (purple), 0.5 (lightblue) and 3 (green) The initial state $|\psi\rangle$ is random state in the even space.

Appendix C: Scaling of the time regimes

The regimes of the error $\epsilon_N(t)$ and of the echo $|\langle\psi_N(t)|\psi(t)\rangle|^2$ of Fig. 2 depend on t_{exp} and t_{coll}. We want to study how these time regimes depend on the dimension N of the Krylov subspace and the number of states D of the Hilbert space of the system. In Fig. 7, t_{coll} (top panel) and t_{exp} (bottom panel) are plotted as a function of N for spin chain of length $L = 6$ (circles) and 10 (squares) [the parameters of the chain are $J = 1$, $h_x = 1$ and $h_z = 0$ (purple symbols), 0.5 (green symbols) and 3 (lightblue symbols)]. These time regimes were computed averaging over 100 initial states and are scaled with the Hilbert norm of the Hamiltonian to avoid spurious dependencies. We can see a smooth quasi-linear dependence of these regimes with N. We also see a small dependency with the Hamiltonian and with the number of states of the Hilbert space. This quasi-linear dependence shows how robust these times are for estimating our bound. Same calculations of t_{coll} and t_{exp} were done for a Hamiltonian with random entries taken from a $\mathcal{N}(0,1)$ distribution (i.e. draw from the Gaussian Unitary Ensemble). This is shown in Fig. 8. We plot t_{coll} (top panel) and t_{exp} (bottom panel) averaging over 100 initial states and are scaled with the Hilbert norm of the Hamiltonian. The Hilbert space dimensions are $D = 64$ (circles) and 1024 (squares.) Again, a clear smooth dependence with N is seen. This guarantees the possibility of using these times to develop a bound to control the error.

Appendix D: Quadratic behaviour of the bound with next hopping coefficient

This appendix is devoted to present the equation Eq. (8) of the main text. Let us suppose first that the chain is in a state where the Krylov approximation is valid, that is, the occupation of the site $N+1$ is close to zero, $|\psi_{K,N+1}|^2(t) \sim 0$. The solution $|\psi_N(t)\rangle$ can be decomposed in the Lanczos basis as a sum of two components,

$$\psi_{N,i}(t) = \psi^{(0)}_{K,i}(t) + \psi^{(1)}_{K,i}(t), \tag{D1}$$

where $\psi^{(0)}_{K,i}(t)$ is the Krylov approximation of order N, that is $\beta_i = 0$ with $i > N$. In the regime where the Krylov approximation holds, it is also valid the relation $|\psi^{(0)}_{K,i}(t)|^2 >> |\psi^{(1)}_{K,i}(t)|^2$ with $i \leq N$. It is straightforward to show the equation of motion for $\psi^{(0)}_{K,i}(t)$,

$$i\frac{d}{dt}\psi^{(0)}_i = \alpha_N\psi^{(0)}_i + \beta_{N-1}\psi^{(0)}_{i-1} + \beta_N\psi^{(0)}_{i+1} \tag{D2}$$

$$\psi^{(0)}_i(t) = 0 \quad if \quad i > N, \tag{D3}$$

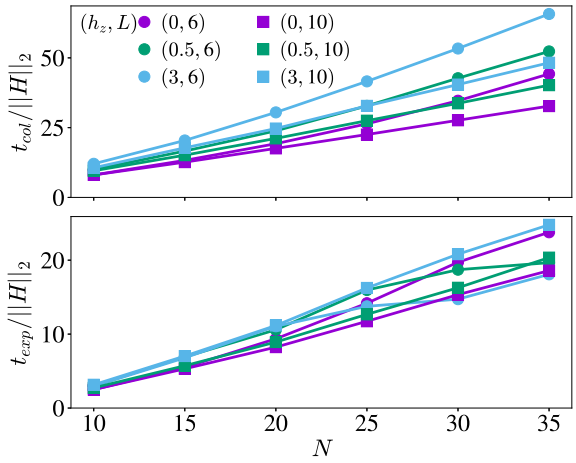

Figure 7. (Upper panel) Scaled t_{col} for the transverse field Ising model with fixed parameter $h_x = 1$ and $h_z = 0$ (purple), 0.5 (green) and 3 (lightblue). The different markers represent chains of length $L = 6$ (circles) and $L = 10$ (squares) with dimensions $D = 64$ and $D = 1024$ respectively. Calculations are done using 100 random initial state conditions in order to smooth out statistical fluctuations (Bottom panel) The same plot but for the scaled t_{exp} quantity.

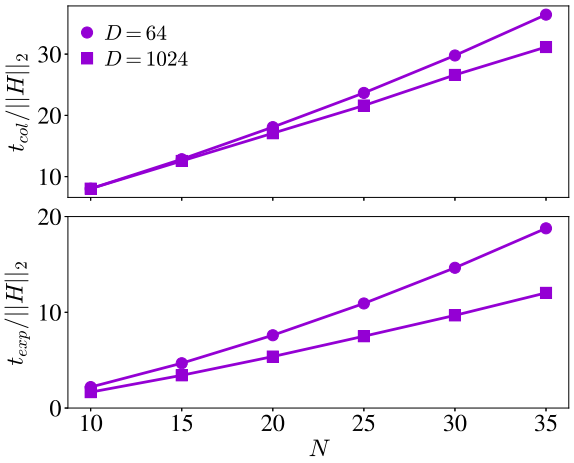

Figure 8. (Upper panel) Scaled t_{col} for a Hamiltonian with random entries taken from a $\mathcal{N}(0, 1)$ distribution. The different markers represent Hamiltonians with dimensions with dimensions $D = 64$ (circles) and $D = 1024$ (squares). Calculations are done using 100 random initial state conditions in order to smooth out statistical fluctuations (Bottom panel) The same plot but for the scaled t_{exp} quantity.

where we have omitted the temporal dependence and the index K of the amplitudes $\psi^{(0)}_{K,i}(t)$. Same simplification of the notation is used in the rest of the appendix. The Schrodinger equation for the full solution is

$$i\frac{d}{dt}\left[\psi_i^{(0)} + \psi_i^{(1)}\right] = \alpha_N\left(\psi_i^{(0)} + \psi_i^{(1)}\right) + \beta_{N-1}\left(\psi_{i-1}^{(0)} + \psi_{i-1}^{(1)}\right) + \beta_N\left(\psi_{i+1}^{(0)} + \psi_{i+1}^{(1)}\right). \tag{D4}$$

We are interested in the Eq. (D4) for $i = N+1$, in this case the terms $\psi^{(0)}_{N+1}$ and $\psi^{(0)}_{N+2}$ vanish. And $|\psi^{(0)}_N| >> |\psi^{(1)}_N|$, then the equation of motion for $\psi^{(1)}_{N+1}$ result in,

$$i\frac{d}{dt}\psi^{(1)}_{N+1} = \alpha_{N+1}\psi^{(1)}_{N+1} + \beta_N\psi^{(0)}_N. \tag{D5}$$

Eq. (D5) can be solve taking the Laplace transform,

$$\hat{\psi}^{(1)}_{N+1} = \beta_N\left\{\frac{\hat{\psi}^{(0)}_N}{is - \alpha_{N+1}}\right\} \tag{D6}$$

and then using some properties of the Laplace transform,

$$\psi^{(1)}_{N+1} = i\beta_N\int_0^t e^{i\alpha_{N+1}t}\psi^{(0)}_N = \beta_N I(t) \tag{D7}$$

The full solution, throwing the order one for the sites $i \leq N$ is,

$$\psi_{N+1,i} = \begin{cases} A\psi_i^{(0)} & i \leq N \\ A\psi_N^{(1)} & i = N \\ 0 & i > N, \end{cases} \tag{D8}$$

with $A = 1/\sqrt{1 + |I(t)|^2\beta_N^2}$ a normalization factor. Then, the overlap between the solution for the Lanczos approximation and the next order is,

$$|\left\langle\psi_K\middle|\tilde{\psi}_{K+1}\right\rangle|^2 = A^2, \tag{D9}$$

where $\tilde{\psi}_{K+1}$ is the solution using $\beta_N = \tilde{\beta}$. Finally, it is straightforward to show,

$$\frac{1 - |\left\langle\psi_K\middle|\tilde{\psi}_{K+1}\right\rangle|^2}{1 - |\left\langle\psi_K|\psi_{K+1}\right\rangle|^2} \sim \frac{1 - \tilde{A}^2}{1 - A^2} \sim \left(\frac{\tilde{\beta}}{\beta}\right)^2. \tag{D10}$$

In the Fig. 9 it is shown the validity of the quadratic behavior of the Eq. (D10) for an Ising spin chain with $L = 10$ sites with $J = 1$, $h_x = 1$ and $h_z = 0.5$ and $T = 25$ (circles), 35 (squares) and 40 (triangles).

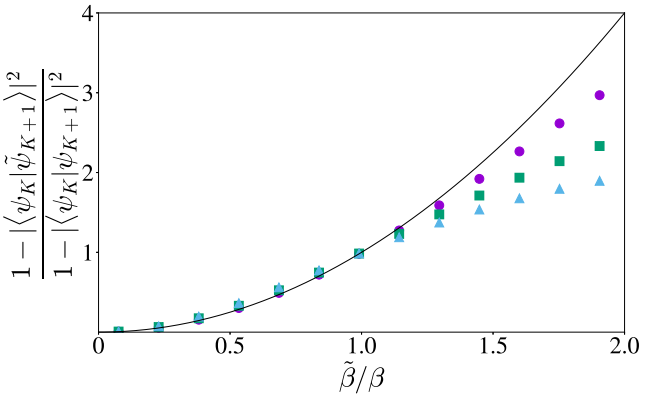

Figure 9. $\frac{1-|\langle\psi_K|\tilde{\psi}_{K+1}\rangle|^2}{1-|\langle\psi_K|\psi_{K+1}\rangle|^2}$ vs. $\frac{\tilde{\beta}}{\beta}$ for an Ising spin chain with $L = 10$ sites with $J = 1$, $h_x = 1$ and $h_z = 0.5$. $T = 25$ (circles), 35 (squares) and 40 (triangles). The function x^2 is plotted with solid line.

Appendix E: Analytical solution of the error: special case of homogeneous hopping

In this appendix, we solve a simplified model for the evolution on the Krylov subspace $\mathcal{K}_N$. Let us assume that after mapping $|\psi\rangle$ and H to $|0\rangle_N$ and T_N, we find a homogeneous tridiagonal matrix,

$$T_N = \alpha \sum_{n=1}^{N} |n\rangle\langle n| + \beta \sum_{n=1}^{N-1} |n\rangle\langle n+1| + \text{h.c.}\,. \tag{E1}$$

Here, $|n\rangle \equiv |n\rangle_N$ (here and hereafter we drop de subscript) denotes the localized "site" states of the N-dimensional tight-binding chain associated with the dynamical system (ψ,H). The Hamiltonian in Eq. (E1) corresponds to the so-called Toeplitz tridiagonal matrix [25–27], and has well documented analytical expressions for its eigenstates and eigenenergies,

$$\langle n|E_k\rangle = \sqrt{\frac{2}{N+1}} \sin\left(\frac{nk\pi}{N+1}\right), \tag{E2}$$

and

$$E_k = \alpha + 2\beta \cos\left(\frac{nk\pi}{N+1}\right). \tag{E3}$$

The time evolution of an arbitrary initial state $|\psi(t=0)\rangle = \sum_{n=1}^{N} c_n |n\rangle$ is given by,

$$|\psi(t)\rangle = \sum_{n,n'}^{N} c_n S^N_{n,n'}(t) |n'\rangle, \tag{E4}$$

where the transition matrix $S^N_{n,n'}(t)$ is defined as,

$$S^N_{n,n'}(t) = \sqrt{\frac{2}{N+1}} \sum_{k=1}^{N} \sin\left(\frac{nk\pi}{N+1}\right) \sin\left(\frac{n'k\pi}{N+1}\right) e^{itE_k}. \tag{E5}$$

Finally, the amplitude of the echo of two time-evolutions with Toeplitz matrices of lengths N and N' yields,

$$\langle 0| e^{-itT'_N} e^{itT_N} |0\rangle = 1 - \sum_{n=1}^{N'} S^N_{1,n}(t) S^{N'}_{n,1}(-t). \tag{E6}$$

It is clear from Eq. (E3), that the parameter α will not affect the value of the echo and β acts as a rescaling of time. Thus, one can limit itself to study the behavior of the chain with parameters $\alpha = 0$ and $\beta = 1$, and then rescale time by βt.

[1] D. Bruss and G. Leuchs, *Quantum Information, 2 Volume Set: From Foundations to Quantum Technology Applications* (John Wiley & Sons, 2019).

[2] S. D. Bartlett, B. C. Sanders, S. L. Braunstein, and K. Nemoto, Efficient classical simulation of continuous variable quantum information processes, Phys. Rev. Lett. **88**, 097904 (2002).

[3] B. M. Terhal and D. P. DiVincenzo, Classical simulation of noninteracting-fermion quantum circuits, Phys. Rev. A **65**, 032325 (2002).

[4] E. Kluk, M. F. Herman, and H. L. Davis, Comparison of the propagation of semiclassical frozen gaussian wave functions with quantum propagation for a highly excited anharmonic oscillator, J. Chem. Phys. **84**, 326 (1986).

[5] U. Schollwöck, The density-matrix renormalization group in the age of matrix product states, Annals of Physics **326**, 96 (2011).

[6] M. Khasin and R. Kosloff, Efficient simulation of quantum evolution using dynamical coarse graining, Phys. Rev. A **78**, 012321 (2008).

[7] A. J. Daley, C. Kollath, U. Schollwöck, and G. Vidal, Time-dependent density-matrix renormalization-group using adaptive effective hilbert spaces, . Stat. Mech.: Theory Exp. **2004**, P04005 (2004).

[8] G. Vidal, Efficient simulation of one-dimensional quantum many-body systems, Phys. Rev. Lett. **93**, 040502 (2004).

[9] Y. Saad, *Iterative methods for sparse linear systems* (SIAM, 2003).

[10] S. Gazzola and M. Sabaté Landman, Krylov methods for inverse problems: Surveying classical, and introducing new, algorithmic approaches, GAMM-Mitteilungen **43**, e202000017 (2020).

[11] T. J. Park and J. Light, Unitary quantum time evolution by iterative lanczos reduction, J. Chem. Phys. **85**, 5870 (1986).

[12] Y. Saad, Analysis of some krylov subspace approximations to the matrix exponential operator, SIAM J. Numer. Anal. **29**, 209 (1992).

[13] D. E. Stewart and T. Leyk, Error estimates for krylov subspace approximations of matrix exponentials, J. Comput. Appl. Math. **72**, 359 (1996).

[14] M. Hochbruck and C. Lubich, On krylov subspace approximations to the matrix exponential operator, SIAM J. Numer. Anal. **34**, 1911 (1997).

[15] R. B. Sidje, Expokit: A software package for computing matrix exponentials, ACM Trans. Math. Softw. **24**, 130–156 (1998).

[16] I. Krupov, Polynomially scaling spin dynamics II: further state-space compression using Krylov subspace techniques and zero track elimination, Journal of Magnetic Resonance **195**, 45 (2008).

[17] C. Moler and C. Van Loan, Nineteen dubious ways to compute the exponential of a matrix, twenty-five years later, SIAM review **45**, 3 (2003).

[18] T. Jawecki, W. Auzinger, and O. Koch, Computable upper error bounds for Krylov approximations to matrix exponentials and associated φ-functions, BIT Numer. Math. **60**, 157 (2020).

[19] A. Goussev, R. A. Jalabert, H. M. Pastawski, and D. A. Wisniacki, Loschmidt echo, Scholarpedia **7**, 11687 (2012).

[20] T. Prosen, T. H. Seligman, and M. Žnidarič, Dynamics of loschmidt echoes and fidelity decay, Physics Reports **435**, 33 (2006).

[21] P. Jacquod and C. Petitjean, Decoherence, entanglement and irreversibility in quantum dynamical systems with few degrees of freedom, Adv. Phys. **58**, 67 (2009).

[22] Th. Guhr, A. Müller–Groeling, and H. A. Weidenmüller, Random-matrix theories in quantum physics: common concepts, Physics Reports **299**, 189 (1997).

[23] J. Ruffinelli, E. Fortes, M. Larocca, and D. A. Wisniacki, in preparation (2021).

[24] A. Edelman and N. R. Rao, Random matrix theory, Acta Numer. **14**, 233 (2005).

[25] S. Noschese, L. Pasquini, and L. Reichel, Tridiagonal toeplitz matrices: Properties and novel applications, Numerical Linear Algebra with Applications **20** (2013).

[26] R. M. Gray, *Toeplitz and circulant matrices: A review* (now publishers inc, 2006).

[27] A. Böttcher and S. M. Grudsky, *Spectral properties of banded Toeplitz matrices* (SIAM, 2005)
.